Impact of key residues within chloroplast thioredoxin-*f* on recognition for reduction and oxidation of target proteins

Received for publication, July 29, 2019, and in revised form, October 2, 2019 Published, Papers in Press, October 9, 2019, DOI 10.1074/jbc.RA119.010401

Yuichi Yokochi[‡§], Kazunori Sugiura[‡], Kazuhiro Takemura[¶], Keisuke Yoshida[‡§], Satoshi Hara[§], Ken-ichi Wakabayashi[‡§], Akio Kitao[¶], and Toru Hisabori[‡§1]

From the [‡]Laboratory for Chemistry and Life Science, Institute of Innovative Research, and [§]School of Life Science and Technology, Tokyo Institute of Technology, Nagatsuta-cho 4259-R1–8, Midori-ku, Yokohama 226-8503, Japan and the [¶]School of Life Science and Technology, Tokyo Institute of Technology, 2-12-1 Ookayama, Meguro, Tokyo 152-8550, Japan

Edited by Joseph M. Jez

Thioredoxin (Trx) is a redox-responsive protein that modulates the activities of its target proteins mostly by reducing their disulfide bonds. In chloroplasts, five Trx isoforms (Trx-*f*, Trx-*m*, Trx-*x*, Trx-*y*, and Trx-*z*) regulate various photosynthesis-related enzymes with distinct target selectivity. To elucidate the determinants of the target selectivity of each Trx isoform, here we investigated the residues responsible for target recognition by Trx-*f*, the most well-studied chloroplast-resident Trx. As reported previously, we found that positively-charged residues on the Trx-*f* surface are involved in the interactions with its targets. Moreover, several residues that are specifically conserved in Trx-*f* (*e.g.* Cys-126 and Thr-158) were also involved in interactions with target proteins. The validity of these residues was examined by the molecular dynamics simulation. In addition, we validated the impact of these key residues on target protein reduction by studying (i) Trx-*m* variants into which we introduced the key residues for Trx-*f* and (ii) Trx-like proteins, named atypical Cys His-rich Trx 1 (ACHT1) and ACHT2a, that also contain these key residues. These artificial or natural protein variants could reduce Trx-*f*–specific targets, indicating that the key residues for Trx-*f* are critical for Trx-*f*–specific target recognition. Furthermore, we demonstrate that ACHT1 and ACHT2a efficiently oxidize some Trx-*f*–specific targets, suggesting that its target selectivity also contributes to the oxidative regulation process. Our results reveal the key residues for Trx-*f*–specific target recognition and uncover ACHT1 and ACHT2a as oxidation factors of their target proteins, providing critical insight into redox regulation of photosynthesis.

Thioredoxin (Trx)[2] is a ubiquitous protein that modulates the activities of various enzymes mostly by reducing disulfide bonds on the target protein molecules. Trx possesses the conserved active-site motif WCGPC, and it also carries a common structure named Trx-fold (1–3). In chloroplasts, Trx modulates the activities of various enzymes involved in photosynthesis-related metabolism (4). Because this process is promoted by the reducing power produced by the light-driven photosynthetic electron transport system, the redox-based regulation system enables plants to adequately adapt to fluctuating light conditions.

Two chloroplast Trxs named Trx-*f* and Trx-*m* were initially identified as activators of fructose-1,6-bisphosphatase (FBPase) and NADP-malate dehydrogenase in chloroplasts, respectively (5–7). Several enzymes, including Calvin-Benson cycle enzymes (glyceraldehyde-3-phosphate dehydrogenase, sedoheptulose-1,7-bisphosphatase, and phosphoribulokinase (4, 8)), glucose-6-phosphate dehydrogenase (9), and chloroplast ATP synthase γ-subunit (10), were then identified as targets of Trx-mediated reduction. In 2000, the whole-genome sequences of the green plant *Arabidopsis thaliana* were revealed (11), and five chloroplast Trx isoforms (*f*-, *m*-, *x*-, *y*-, and *z*-type) were identified in the genome based on their sequence similarities. In addition, the plant genome data enabled us to study unknown Trx–targeted proteins via various proteomic approaches such as two-dimensional SDS-PAGE analysis, following chemical modification of free thiols, and affinity chromatography using the immobilized monocysteine mutant Trx (12–15). These approaches explosively increased the number of Trx–targeted proteins.

Chloroplast Trxs specifically recognize their targets. For example, Trx-*f* appeared to preferentially reduce proteins involved in the Calvin-Benson cycle such as FBPase and CP12, whereas other Trx isoforms in chloroplasts cannot efficiently reduce these proteins (6–8, 16–19). However, the determinant of the target selectivity of Trx-*f* and the differences among the determinants of Trx isoforms are not known very well.

This work was supported by JSPS KAKENHI Grant 16H06556 (to T. H.), by Dynamic Alliance for Open Innovation Bridging Human, Environment, and Materials, by MEXT/JSPS KAKENHI Grants JP17KT0026 and JP19H03191 (to A. K.), and by MEXT Priority Issues on Post-K Computer Projects "Building Innovative Drug Discovery Infrastructure through Functional Control of Biomolecular System" (to A. K.). The authors declare that they have no conflicts of interest with the contents of this article.

This article contains Fig. S1, Tables S1 and S2, and supporting Movies S1–S3.

[1] To whom correspondence should be addressed: Laboratory for Chemistry and Life Science, Institute of Innovative Research, Tokyo Institute of Technology, Nagatsuta-cho 4259-R1-8, Midori-ku, Yokohama 226-8503, Japan. Tel.: 81-45-924-5234; Fax: 81-45-924-5268; E-mail: thisabor@res.titech.ac.jp.

[2] The abbreviations used are: Trx, thioredoxin; TrxR, Trx reductase; FBPase, fructose-1,6-bisphosphatase; FRET, Förster resonance energy transfer; SEC, size-exclusion chromatography; HIC, hydrophobic-interaction chromatography; PDB, Protein Data Bank; NTRC, NADPH-Trx reductase C; ACHT, atypical Cys His-rich Trx; Prx, peroxiredoxin; CEC, cation-exchange chromatography; TrxL2, Trx-like 2; MD, molecular dynamics.

© 2019 Yokochi et al. Published under exclusive license by The American Society for Biochemistry and Molecular Biology, Inc.

The midpoint redox potentials (E_m) of the redox-responsive cysteine pairs on Trx and its target molecules are some of the factors determining the direction of the reactions (20). In addition, a relationship between the E_m values of chloroplast Trxs and the rates of electron transfer from their reductase to Trxs was also reported (21). However, the target selectivity of each chloroplast Trx isoform is apparently irrelevant to its E_m (16, 18, 21, 22). For example, Trx-*f* and Trx-*m* have similar E_m values, but only Trx-*f* can efficiently reduce FBPase (18). These Trx-dependent reduction processes were found to be rate-limiting steps in the light-dependent activation of chloroplast enzymes (23). Thus, target selectivity might determine the activation rate of each enzyme and enable the sophisticated regulation of various chloroplast functions.

To elucidate the determinant of the target selectivity of Trx-*f*, several mutational and kinetic analyses have been conducted (24–28). These previous studies were mostly based on only the differences among Trx-*f* and -*m* from spinach and Trx from *Escherichia coli*. In addition, other Trxs (Trx-*x*, Trx-*y*, and Trx-*z*) were not considered at that time because they were not identified before the *A. thaliana* whole-genome analysis (16, 29, 30). Thus, the determinants of the target selectivity of Trx isoforms have not been completely identified. To address this question, we studied the residues specifically conserved in Trx-*f* via comparisons of the amino acid sequences of chloroplast Trxs from various plants. Some of the conserved residues should be candidate residues that are involved in Trx-*f*–specific target recognition. We then adopted a recently-developed sensor protein that can detect the reduction of a targeted protein of Trx-*f* as a fluorescent signal. This Förster resonance energy transfer (FRET)-based sensor protein, which is named "change in redox state of thioredoxin 1 (CROST1)" (31), is useful for studying the efficiency of reducing power transfer from Trx-*f* to the target. Using this new sensor protein and various site-directed mutants of Trxs, we could identify the key residues as the determinant of the target selectivity of Trx-*f*.

We recently identified Trx-like 2 (TrxL2) as a critical protein for the oxidation process of Trx–targeted proteins in chloroplasts (32). A similar result was reported previously (33) regarding atypical Cys His-rich Trx 4 (ACHT4), which is also a Trx-like protein. In this study, we found that ACHT1 and ACHT2 also possess the key residues, which were identified on Trx-*f*, based on the sequence comparison. We then demonstrated the function of these residues during the target oxidation process.

Results

Specific residues conserved in each type of chloroplast Trxs

Ten chloroplast Trx isoforms, which were designated as Trx-*f*1, Trx-*f*2, Trx-*m*1, Trx-*m*2, Trx-*m*3, Trx-*m*4, Trx-*x*, Trx-*y*1, Trx-*y*2, and Trx-*z*, were found in *A. thaliana* (19). The orthologs of these Trx genes were also identified in other plant genomes via sequence similarity–based surveys (34, 35). To explore the residues potentially involved in the target selectivity of each type of Trxs, we first conducted an amino acid sequence comparison of Trxs from several plants that are well-annotated in the UniprotKB database. We also included well-studied *Chlamydomonas* Trxs, although the Trx system in *Chlamydomonas* is somewhat different from those of vascular plants (8, 35). Consequently, 14 residues were identified as candidate residues responsible for the target selectivity of Trx-*f* (Fig. 1, *A–C*, highlighted in *magenta*). Notably, most of the specific residues for each type of Trxs were located on the surface of the molecule, which presumably can interact with target proteins (see residues highlighted in *magenta* or *black* and the *Interaction interface line* in Fig. 1*A*, as well as *B–D*).

Decrease of the target reduction activity via mutation of Trx-f–distinctive residues

We then prepared various Trx-*f*1 mutants harboring mutations of Trx-*f*–distinctive residues (Fig. 1*B*). Five amino acid residues of Trx-*f*1 (Met-94, Thr-96, Asn-127, Leu-137, and Asn-151) were replaced by their counterparts in the other types of Trxs because they are mostly conserved as other amino acid residues in the other types of Trxs (Fig. 1*A*). Seven hydrophilic residues of Trx-*f*1 (Gln-97, Asp-118, Arg-131, Lys-135, Glu-156, Thr-158, and Lys-161) were substituted with Ala, and one hydrophobic residue (Val-141) was replaced by Ser. Cys-126 was substituted with both Ser and Ala. Because Val-142 is located at the *cis*-Pro−1 position (Fig. 1*A*, *asterisk*) and the amino acid at this position is reported to be important for the redox property of Trx-family proteins (20), we also introduced a mutation in this residue (see "Discussion" for details). However, all residues at this position of chloroplast Trxs have a similar hydrophobic property. We therefore replaced Val-142 with Met because Met is found at this position in TrxL2 (35), which could not efficiently reduce Trx-*f*–specific targets in our previous study (32). Trx-*f*1 mutants expressed in *E. coli* were then purified to homogeneity, although the mutants for Met-94, Asp-118, and Leu-137 were not obtained as soluble proteins.

To confirm the activity of the purified Trx-*f*1 mutants as reductants, we evaluated their E_m values and insulin-reducing activities (36) in the presence of reduced dithiothreitol (DTT). The E_m value for the wildtype (WT) Trx-*f*1 is reported to be −321 mV at pH 7.5 (18). Indeed, half of WT Trx-*f*1 was reduced in the buffer with the redox potential −321 mV (Fig. 2*A*). In this redox buffer, the ratio of the reduced fractions of most of Trx-*f*1 mutants was around 0.5, indicating that their E_m values are similar to that of WT Trx-*f*1. So far, the E_m values of *A. thaliana* chloroplast Trx isoforms are reported to be within the range from −335 to −276 mV at pH 7.5 (18, 21). As shown in Fig. 2*A*, the ratio of the reduced fractions of all Trx-*f*1 mutants was higher than 0.5 at redox potential −335 mV and lower than 0.5 at redox potential −276 mV. These results clearly demonstrate that E_m values of Trx-*f*1 mutants are in the range of those of typical chloroplast Trxs. Insulin-reducing activity measurement shows that all examined mutants retained more than 85% of the activity of WT Trx-*f*1 (Fig. 2, *B* and *C*). These results indicate that the residues of Trx-*f*1 examined in this study are not strongly involved in the redox properties of Trx, namely the reductase activity.

Subsequently, we examined the reduction activities of these mutants using the typical *f*-type Trx-specific target enzyme FBPase. To confirm that the residues are important not only for FBPase recognition but also for other Trx-*f*–specific targets, we

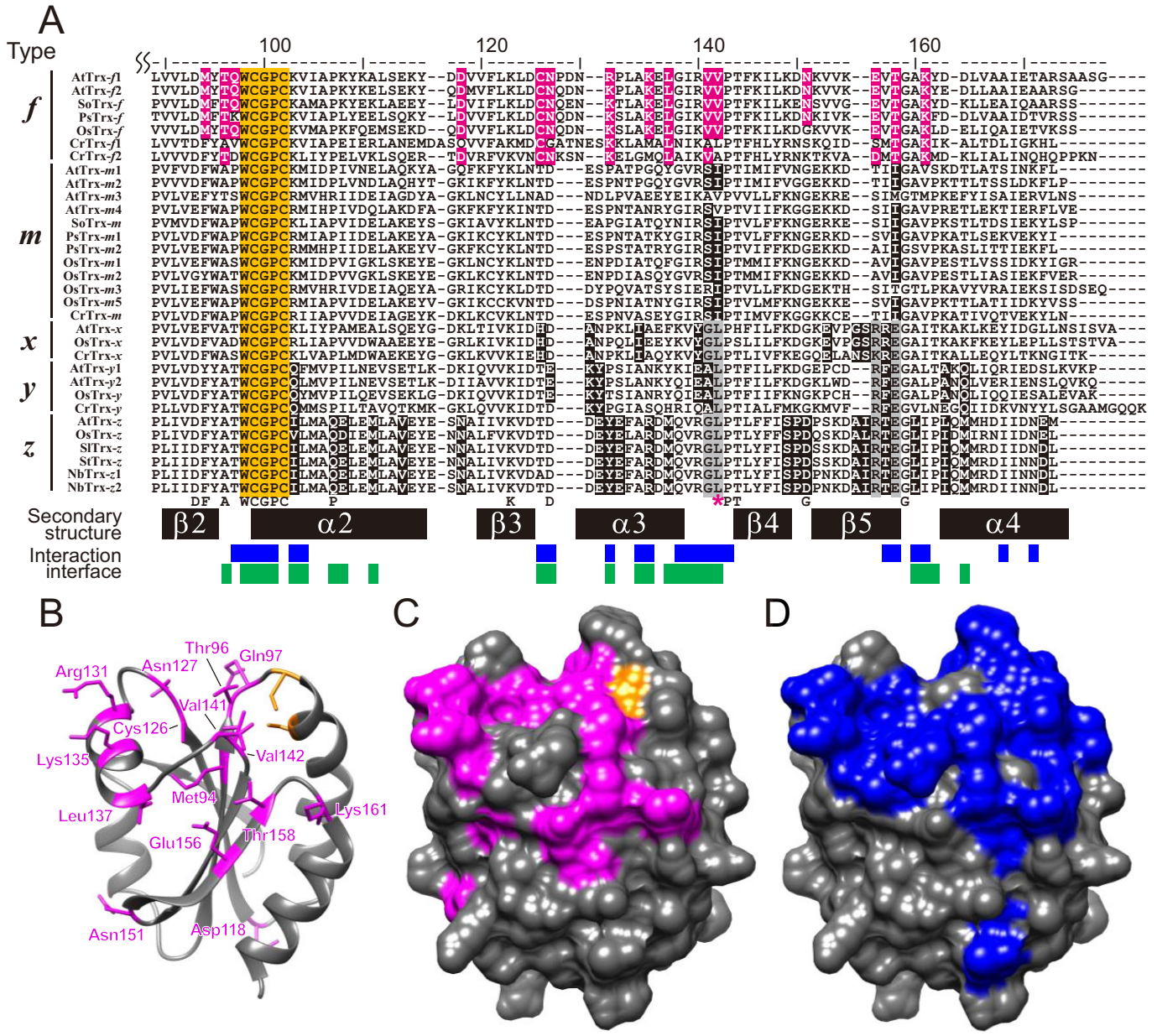

Figure 1. Residues specifically conserved in each type of Trxs. *A,* amino acid sequence comparison of chloroplast Trxs from various plants. In the alignment result, the type-specific residues, active-site residues, and residues conserved among Trx-*x*, Trx-*y*, and Trx-*z* are highlighted in *magenta* or *black, orange*, and *gray*, respectively. The residue numbers of *A. thaliana* Trx-*f*1 (counted from the translational start site amino acid methionine) are shown *above the figure*. *Each letter* and *an asterisk below* the alignment result denote conserved residues in typical Trxs (2) and the *cis*-Pro−1 residue (20), respectively. The secondary structure of SoTrx-*f* (PDB code 1F9M) is shown on the *Secondary structure line*. On the *Interaction interface line*, the residues of Trxs that are predicted to interact with target proteins (*upper, blue*) or Trx reductases (*bottom, green*) are shown. Full names of the organisms are described in Table S1. *B–D,* model structure of *A. thaliana* Trx-*f*1. Trx-*f*–specific residues (*magenta*) and Cys residues in the active site (*orange*) (*B* and *C*), residues involved in the interaction with targets (*blue*) (*D*) are shown in a ribbon or molecular surface model.

used the artificial Trx-*f*–specific target protein CROST1 as well. CROST1 is a FRET-based sensor protein constructed using cyan fluorescent protein, yellow fluorescent protein, and the N-terminal region of CP12, a redox-sensitive regulator protein of the Calvin-Benson cycle. The reduction of CROST1 is easily assessed via its fluorescent signal, and the redox status of Trx-*f* was successfully monitored *in vivo* using this sensor protein (31). The reduction activities of Trx mutants were assessed by analyzing the rate constants of target protein reduction (see "Experimental procedures"). Consequently, most of the mutations in Trx-*f*1 significantly decreased their reduction activities, particularly for FBPase reduction (Fig. 3). One exception was the mutant N151G, which exhibited a similar ability to reduce target proteins as WT. Based on these results, we concluded that the Trx-*f*– distinctive residues shown in Fig. 1, *A* and *B*, excluding Met-94, Asp-118, Leu-137, and Asn-151 are the key residues for the target selectivity of Trx-*f*.

Interaction between Trx-f and FBPase in a dynamic structural model

To evaluate the validity of these key residues for target recognition, the interaction between Trx-*f* and FBPase was

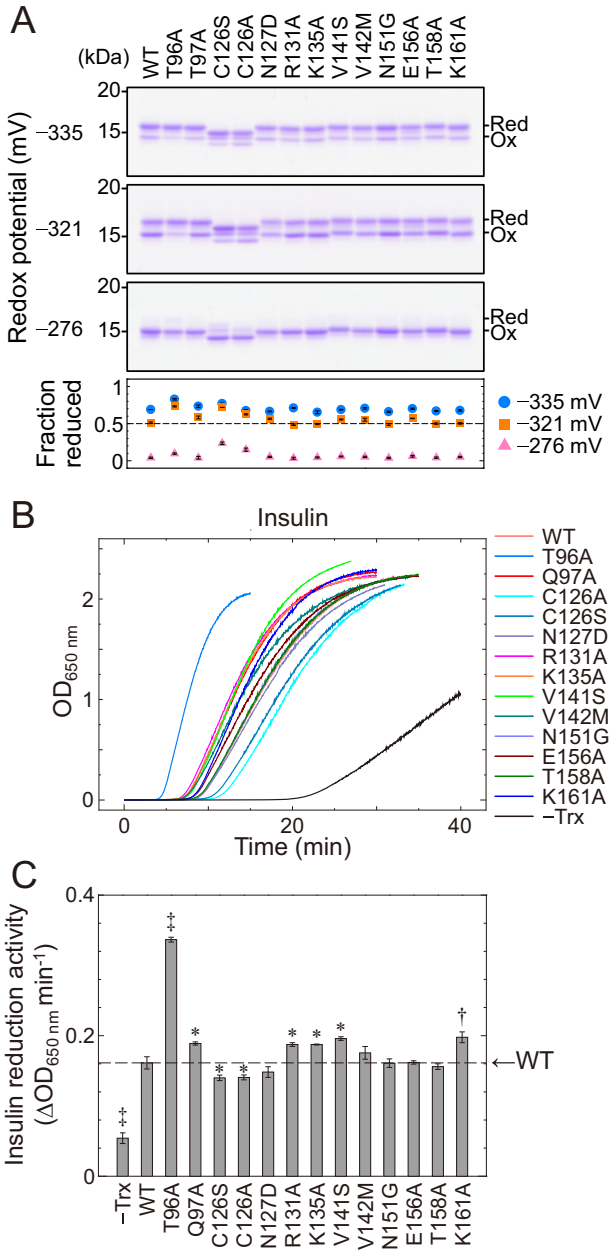

Figure 2. Redox properties of *A. thaliana* Trx-*f*1 variants. *A*, E_m range of Trx-*f*1 variants. Each variant was incubated in the buffer containing 50 mM oxidized DTT and 9, 3, and 0.09 mM reduced DTT, whose redox potential values are −335, −321, and −276 mV at pH 7.5, respectively. Other conditions are same as those for determination of E_m described under "Experimental procedures." Reduced (*Red*) and oxidized (*Ox*) Trxs were discriminated via the thiol group modification using 4-acetamido-4′-maleimidylstilbene-2,2′-disulfonate followed by SDS-PAGE. Values of reduced fractions are presented as the mean ± S.D. ($n = 3$). *B*, time-dependent insulin reduction by Trx-*f*1 variants. In the presence of 0.5 mM reduced DTT, 230 μM bovine insulin was incubated with 5 μM Trx-*f*1 variants. Turbidity resulting from reduced insulin was monitored at 650 nm. *C*, insulin reduction activities of Trx-*f*1 variants. The activity of each variant was determined by linear regression of the data shown in *B*. Values are presented as the mean ± S.D. ($n = 3$). *Each symbol* indicates a significant difference (*, $p < 0.05$; †, $p < 0.01$; ‡, $p < 0.001$; Welch's *t* test) between the designated value and the value of WT Trx-*f*1.

examined in a structural model of their complex. To explore a feasible complex structure, we generated a large number of protein/protein complex models by docking, and we selected reasonable models based on Cys residue distances followed by molecular dynamics (MD) simulations. Consequently, we could obtain a dynamic structural model of a Trx-*f*/FBPase complex (Movies S1–S3) and a representative structural model of the complex (Fig. 4*A*). Based on this structural model, minimum pairwise heavy atom distance between each of the Trx-*f* key residues and FBPase (d_{min}) was determined (Fig. 4*B*). Assuming that residues whose d_{min} values are less than 4 Å interact with FBPase, Thr-96, Arg-131, Val-141, and Val-142 almost constantly interact with FBPase, whereas d_{min} values of the other Trx-*f*–distinctive residues were found to oscillate significantly (Fig. 4*B* and Movies S1–S3). According to these results, most of the key residues for Trx-*f* are supposed to interact with a target protein concomitantly with continuous conformational changes.

Introduction of the key residues for Trx-f into Trx-m2

Next, we validated the impact of the key residues for Trx-*f* on Trx-*f*–specific target recognition using Trx-*m*2 mutants. For this purpose, the identified key residues were divided into four groups, and they were substituted into the corresponding parts of Trx-*m*2. The mutants Trx-$m2_{T135C/D136N/P139R/G143K}$ (Trx-$m2_{f135-143}$), Trx-$m2_{S152V/I153V}$ (Trx-$m2_{f152-153}$), and Trx-$m2_{T167E/I169T/V172K}$ (Trx-$m2_{f167-172}$) were successfully expressed in *E. coli* and purified, whereas Trx-$m2_{A104T/P105Q}$ was not well-purified because of its insolubility. The mutant Trx-$m2_{T135C/D136N/P139R/G143K/S152V/I153V/T167E/I169T/V172K}$ (Trx-$m2_{f135-172}$) was also prepared to assess the impact of all key residues for Trx-*f* excluding residues corresponding to Ala-104 and Pro-105. Reduction of CROST1 was then examined as FRET signals using these mutants (Fig. 5*A*). The activities of Trx-$m2_{f135-143}$, Trx-$m2_{f167-172}$, and Trx-$m2_{f135-172}$ were significantly higher than that of Trx–$m2_{WT}$ (the fold changes were 40, 4.1, and 56, respectively, when the value of "−Trx" was used as a base) (Fig. 5*B*). A similar tendency was observed for FBPase reduction (Fig. 5*C*). Taken together, these results indicate that the key residues for Trx-*f* play a critical role in the interaction between Trx-*f* and its target proteins.

Reduction of Trx-f–specific target proteins by ACHT1 and ACHT2a

Based on the amino acid sequence comparison of chloroplast Trxs and Trx-like proteins in *A. thaliana*, we found that ACHT1 and ACHT2a partially maintain the key residues identified on Trx-*f*, whereas ACHT4a, another isoform of ACHT, lacks several key residues that are maintained in ACHT1 and ACHT2a (Fig. 5*D*). The reduction activities of these ACHTs against CROST1 and FBPase were then examined. As shown in Fig. 5, *B* and *E*, CROST1 and FBPase were sufficiently reduced by both ACHT1 and ACHT2a, whereas ACHT4a could not reduce either protein. These results clearly demonstrate that these key residues contribute to the interaction with Trx-*f*–specific target proteins.

Efficient oxidation of Trx-f target proteins by ACHT1 and ACHT2a

Although ACHT1 and ACHT2a could reduce Trx-*f*–specific target proteins, their efficiencies were lower than that of Trx-*f*1, and rate constants of Trx-*f*1, ACHT1, and ACHT2a for CROST1 reduction were calculated to be 23.8, 5.16, and 6.22 $\mu M^{-1}\,min^{-1}$, respectively (Fig. 5, *B* and *E*). To clarify the differ-

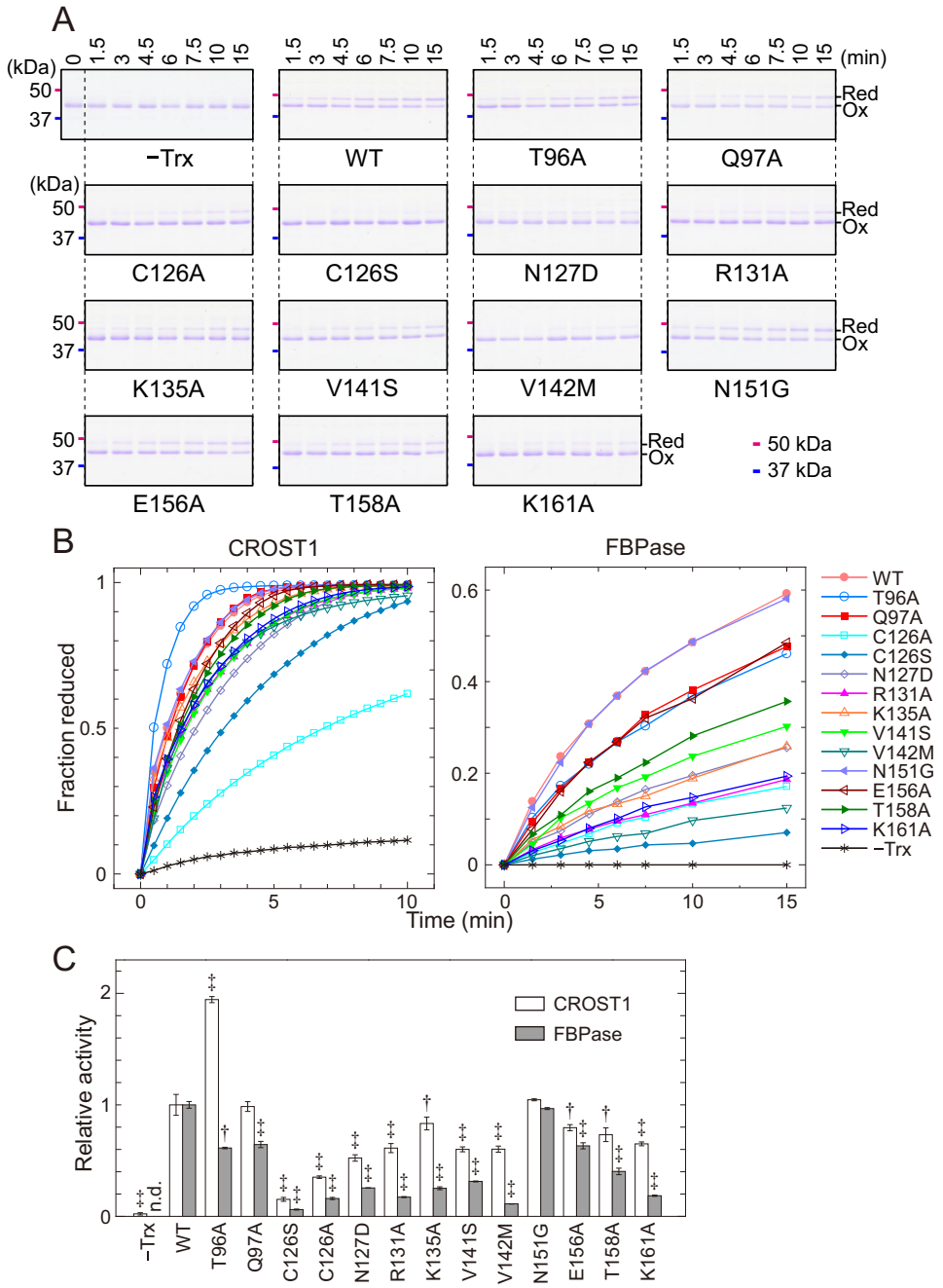

Figure 3. Trx-*f*–specific target reduction activities of Trx-*f*1 variants. *A,* determination of the redox state of FBPase reduced by Trx-*f*1 variants. In the presence of 0.5 mM DTT, 1 μM FBPase was incubated with 0.1 μM Trx and precipitated at each time point. Reduced (*Red*) and oxidized (*Ox*) Trxs were discriminated via the thiol group modification using 4-acetamido-4′-maleimidylstilbene-2,2′-disulfonate followed by SDS-PAGE. *Magenta* and *blue bars* at *the left side of each gel image* indicate molecular mass markers of 50 and 37 kDa, respectively. *B,* time-dependent reduction of CROST1 and FBPase. In the presence of 0.1 mM DTT, CROST1 (0.1 μM) reduction by 0.03 μM Trx was monitored by measuring the FRET intensity as described under "Experimental procedures." Redox state of FBPase was determined in *A* and plotted. For the clarity, the graphs do not include error bars. The graphs with error bars are shown in Fig. S1. *C,* comparison of the Trx-*f*–specific target reduction activities of Trx-*f*1 variants. Reduction activity (μM^{-1} min^{-1}) was determined by fitting the data of *B* to the pseudo first-order Equation 1. The obtained values were then normalized using the value of each WT Trx-*f*1 activity (CROST1: 23.8 μM^{-1} min^{-1}; FBPase: 0.862 μM^{-1} min^{-1}) and are presented as the mean ± S.D. ($n \geq 3$). Each symbol indicates a significant difference (†, $p < 0.01$; ‡, $p < 0.001$; Welch's *t* test) between the designated value and the value of WT Trx-*f*1. *n.d.,* not detected.

ence of the reduction efficiencies of these proteins, we determined the E_m values of ACHTs. This E_m determination was performed under the same conditions described in the previous reports (18, 21, 32) to compare the obtained values with the values of other Trxs in these reports. As shown in Fig. 6*A*, values of −252 and −247 mV were obtained for ACHT1 and ACHT2a at pH 7.5, respectively. The E_m value of ACHT4a was not determined because of the multiple band-shift patterns (Fig. 6*B*). The obtained E_m values of ACHT1 and ACHT2a were markedly higher than those of typical Trxs and moderate between those of TrxL2.1 and TrxL2.2 (Fig. 6*C*) (18, 21, 32), which are two isoforms of TrxL2. These results raised the possibility that ACHT1 and ACHT2a act as oxidation factors similarly as TrxL2 proteins (32).

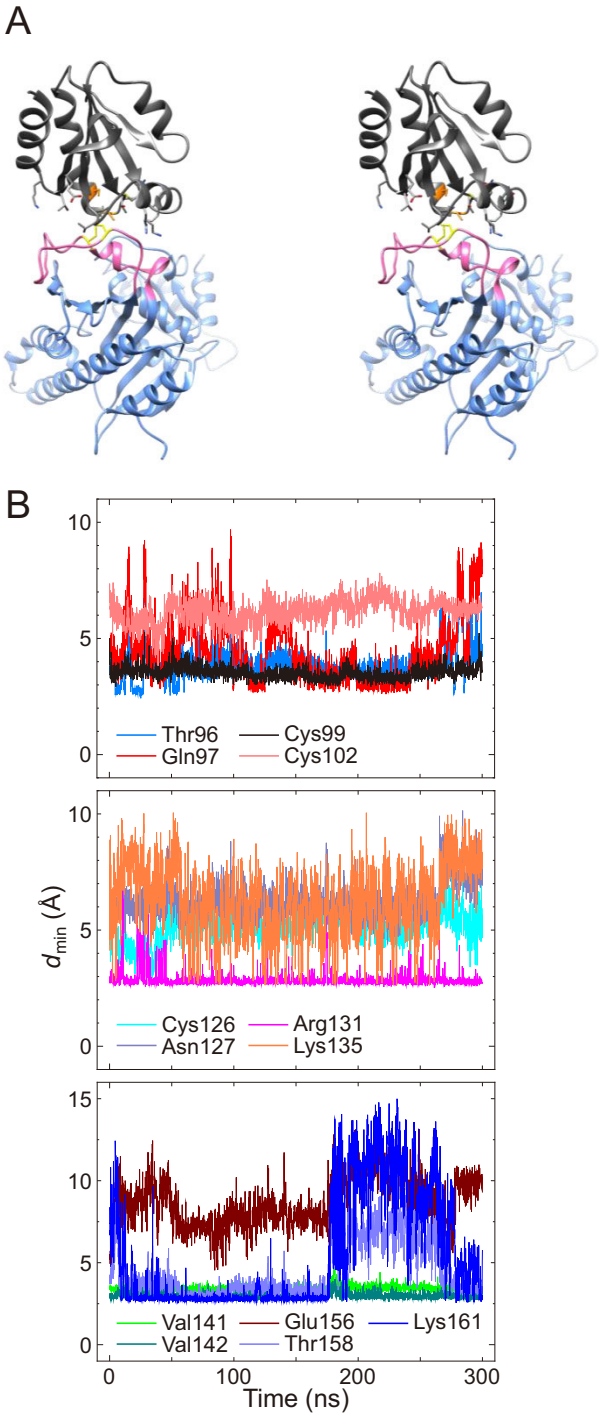

Figure 4. MD simulations of the model structure of Trx-*f*1/FBPase complex. *A,* stereo view of a Trx-*f*1/FBPase complex. *Dark gray* and *cyan* molecules are Trx-*f*1 and FBPase, respectively. The regulatory loop of FBPase and redox-active Cys residues of Trx and FBPase are highlighted in *pink, orange*, and *yellow*, respectively. Atoms and bonds of the key residues for Trx-*f* and redox-active Cys residues are shown. Residue numbers are shown in Movies S1–S3. *B,* time evolution of smallest pairwise heavy atom distances between the key residues of Trx-*f* and any residue of FBPase (d_{min}).

We therefore examined whether ACHT proteins could oxidize CROST1 and FBPase. Consequently, both ACHT1 and ACHT2a oxidized CROST1 more efficiently than Trx-*f*1 (Fig. 7*A*). Oxidation of CROST1 was more obvious after 30 s in the presence of 0.1 μM ACHT1 and ACHT2a than in the presence of 1 μM Trx-*f*1 as indicated in Fig. 7*A*. This implies that oxidation of CROST1 by ACHT1 and ACHT2a occurred at least 10-fold faster than that by Trx-*f*1. In addition, partial re-reduction of the oxidized CROST1 was observed. Because the E_m value of CROST1 was −266 mV (31), which was not significantly different from those of ACHT1 and ACHT2a, these proteins might have remained in a redox equilibrium state in the reaction mixture. FBPase was also efficiently oxidized by ACHT1 and ACHT2a concomitant with their reduction (Fig. 7, *B* and *C*). When the oxidation of FBPase was examined with Trx-*f*1, ~60% of the enzyme was oxidized, but the time required to reach the equilibrium state was less than 30 s, as observed for ACHT1 and ACHT2a. ACHT4a was also able to oxidize these targets, although the oxidation rate was extremely slow.

If ACHT1 and ACHT2a can serve as oxidation factors, then they should drain electrons to a certain acceptor similarly as TrxL2 (32). We therefore examined the capacity of ACHT1 and ACHT2a to reduce 2-Cys peroxiredoxin A (2-Cys PrxA) and PrxQ. Efficient H_2O_2 reduction was observed when ACHT1 and ACHT2a were added to 2-Cys PrxA in the presence of DTT (Fig. 8). Conversely, these reductants could not work with PrxQ, suggesting that ACHT proteins transfer reducing power from their targets to H_2O_2 via 2-Cys Prx in chloroplasts.

Discussion

On the reduction process

Previous studies have largely expanded knowledge on the target selectivity of chloroplast Trxs (16, 18, 29). The determinants of the target selectivity of Trx have also been studied (24–28). However, they have been hardly clarified to date because of the variety of the important residues they suggested. In addition, some of them are not conserved in plant Trx-*f*. For example, Geck *et al.* (25) identified several amino acid residues involved in target recognition by spinach Trx-*f*. One of the critical residues identified in their study was Lys-58 (corresponding to Ala-111 in *A. thaliana* Trx-*f*1). However, this residue was not conserved in other Trx-*f* proteins and was even found in several Trx-*m* isoforms (Fig. 1*A*), implying that this residue should not be a common target recognition residue in Trx-*f*. To reveal the general characteristics of Trx-*f*, we first performed a sequence comparison of Trx proteins from various plants and identified the residues that are specifically conserved in each type of Trx isoforms (Fig. 1*A*). We then found that most of the specific residues are located in the putative interaction interface between Trx and target proteins (Fig. 1). Although the co-crystal structures of chloroplast Trxs with target proteins have not been reported, the Trx–target interaction interface can be predicted using the co-crystal or NMR structures of Trx and target proteins from other origins. The interaction interface between Trx and Trx reductase (TrxR) was also predicted, and it appeared to mostly overlap with the Trx–target interaction interface (Fig. 1*A*, *blue bars* and *green bars*). These results suggest that residues specifically conserved in each type of Trx can be involved in both target and TrxR recognition, although we previously demonstrated that the rate of chloroplast Trx reduction by TrxR correlates with E_m (21).

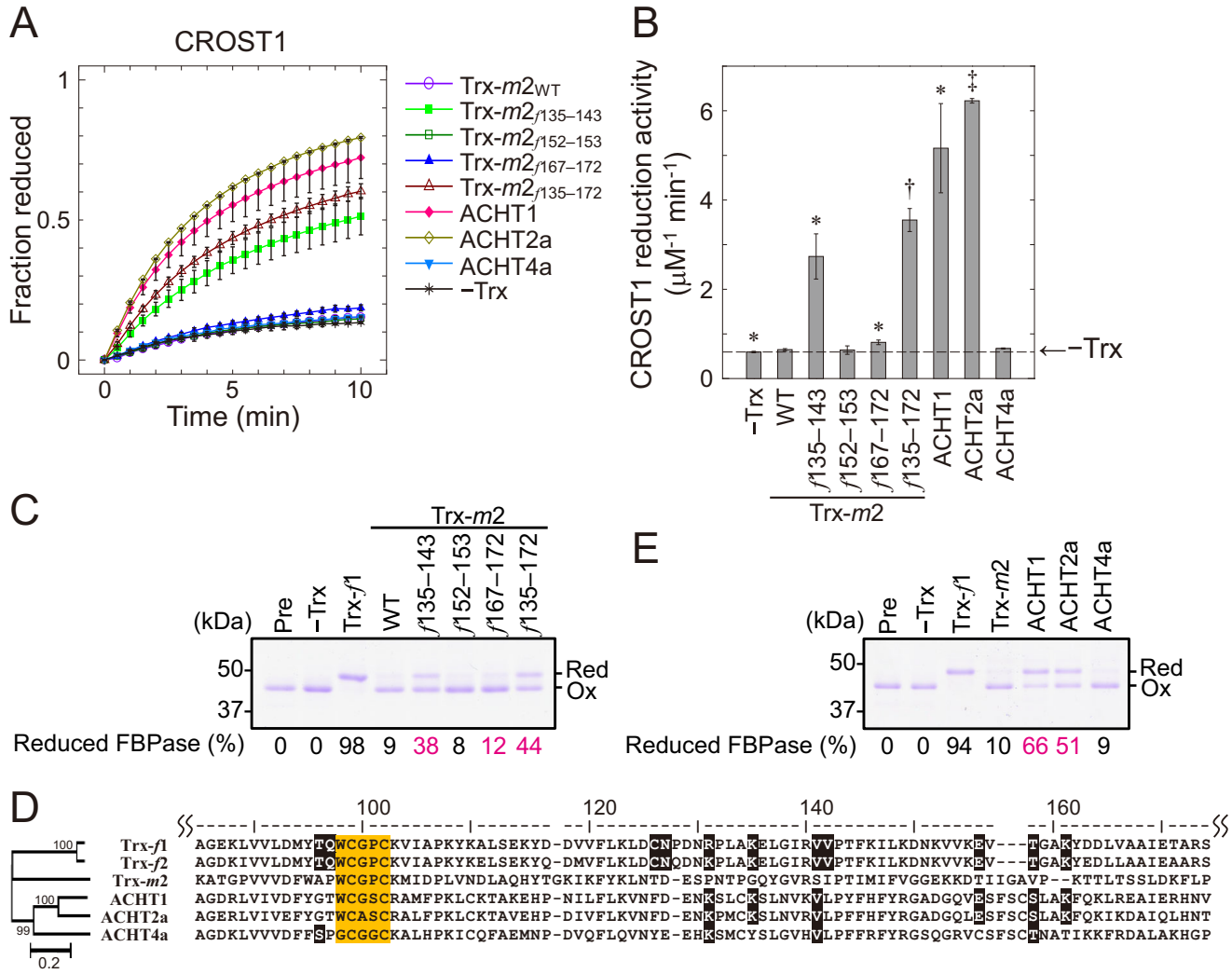

Figure 5. Trx-*f*–specific target reduction activities of Trx-*m*2 variants and ACHT proteins. *A*, time-dependent CROST1 reduction by Trx-*m*2 variants and ACHT proteins. In the presence of 0.1 mM DTT, CROST1 (0.1 μM) reduction by 0.03 μM Trx or ACHT was monitored by measuring the FRET intensity as described under "Experimental procedures." *B*, CROST1 reduction activities of Trx-*m*2 variants and ACHT proteins. Activity (μM^{-1} min^{-1}) was determined by fitting the data of *A* to the pseudo first-order Equation 1, and data are presented as the mean ± S.D. ($n = 3$). Each *symbol* indicates a significant difference (*, $p < 0.05$; †, $p < 0.01$; ‡, $p < 0.001$; Welch's *t* test) between the designated value and that of Trx-$m2_{WT}$. *C*, FBPase reduction activities of Trx-*m*2 variants. After 30 min of incubation of 1 μM oxidized (*Ox*) FBPase with 2 μM Trx in the presence of 0.5 mM reduced (*Red*) form of DTT, the fraction of reduced FBPase was determined via a thiol group modification-based method followed by band intensity measurement. *D*, amino acid sequence comparison of *A. thaliana* Trx-*f*1, Trx-*f*2, Trx-*m*2, and ACHT proteins. The key residues for Trx-*f* and the active-site residues are highlighted in *black* and *orange*, respectively. Residue numbers of *A. thaliana* Trx-*f*1 (counted from the translational start site amino acid methionine) are shown *above the figure*. The phylogenetic tree is shown with bootstrap values (%). *E*, FBPase reduction activities of ACHT proteins. FBPase reduction by ACHT proteins was monitored as described in *C*.

The specific residues in each type of Trx isoforms were observed even at the positions in which residues should be universally conserved among Trx isoforms (*letters shown below the alignment* in Fig. 1*A*) (2). In particular, the *cis*-Pro−1 residue (shown in Fig. 1*A* with an *asterisk*), which is reported to be Ile in many Trx isoforms (20), is Val in Trx-*f*; Ile in Trx-*m*; Leu in Trx-*x*, Trx-*y*, Trx-*z*, and ACHT; and Met in TrxL2 (Figs. 1*A*, 5*D*, and 9, *A* and *B*). Other Trx-like proteins also have specific *cis*-Pro−1 residues, *e.g.* the Trx domain of NADPH-Trx reductase C (NTRC) has Thr at this position (Fig. 9*C*, highlighted in *magenta*). The residue at this *cis*-Pro−1 position is reported to greatly affect the redox properties of the Trx-family proteins (20). We therefore included this residue in the candidates of the key residue for Trx-*f*. The information on the specific residues in each type of Trx isoforms identified in this study might provide insights into the target selectivity of various isoforms, such as the Trx-*y*–specific activation of monodehydroascorbate reductase (37).

Interestingly, several residues of Trx-*z* that are predicted to be involved in target recognition are not located in the interaction interface (see *Type-z* and *Interaction interface lines* in Fig. 1*A*). This might be a unique feature of Trx-*z* because this isoform is suggested to serve as one of the components of plastid-encoded RNA polymerase complex in addition to functioning as a redox mediator (30, 38–41).

In this study, we assessed the impact of the Trx-*f*–distinctive residues on the interaction with Trx-*f*–specific targets via three strategies: (i) evaluation of the target reduction activity of Trx-*f*1 mutants containing a mutation at each Trx-*f*– distinctive residue; (ii) evaluation of the target reduc-

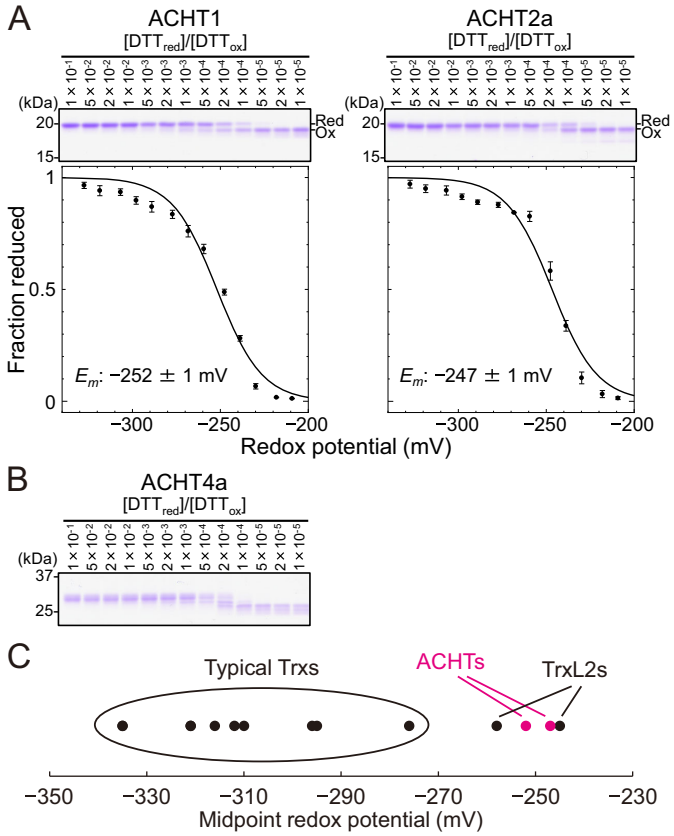

Figure 6. E_m values of ACHT proteins. *A* and *B*, redox titration of ACHT proteins. The SDS-polyacrylamide gel images of redox titration are shown with the molar ratio of reduced and oxidized form of DTT. Reduced (*Red*) and oxidized (*Ox*) ACHT proteins were discriminated via the thiol group modification using 4-acetamido-4′-maleimidylstilbene-2,2′-disulfonate followed by SDS-PAGE. *A*, data obtained from the gel image were fitted to the Nernst equation, and the E_m values of ACHT1 and ACHT2a were determined. All data, including E_m values, are presented as the mean ± S.D. ($n = 3$). *B*, E_m of ACHT4a was not determined because multiple band-shift patterns appeared, and the redox states could not be assigned. *C*, E_m values of typical Trx, TrxL2, and ACHT proteins at pH 7.5. The E_m values of typical Trx and TrxL2 proteins were determined in our previous research (18, 21, 32), and those of ACHT proteins determined in this study are summarized. These E_m values were determined by using the same method.

tion activity of Trx-*m*2 mutants containing some of the Trx-*f*–distinctive residues; and (iii) evaluation of the target reduction activities of ACHT1 and ACHT2a, two Trx-like proteins that possess the Trx-*f*–distinctive residues. The results obtained from the strategy i indicate that most of the Trx-*f*–distinctive residues were crucial for the reduction of Trx-*f*–specific targets, whereas these residues did not greatly affect the reduction capacity of Trx itself (Figs. 2 and 3). In this experiment, mutation at Asn-151 did not alter the reduction activities of Trx-*f*. This result is consistent with the fact that Asn-151 is found at the opposite surface from the position of the active site in the molecule (Fig. 1*B*). The negatively-charged molecular surface around the regulatory Cys residues of targets was reported to be preferentially recognized by the compatible positively-charged surface of Trx-*f* (24–26, 28, 42, 43). These observations are consistent with our finding that the key residues for Trx-*f* contain positively charged residues compared with the other types of Trxs. In addition to these positively-charged residues, we demonstrated that most of the residues that are specifically conserved in Trx-*f* are involved in target recognition. The results of MD simulations clearly show these interactions (Fig. 4 and Movies S1–S3). Although a rigid-body docking simulation of Trx-*f* and FBPase has already been conducted (43), their interaction should be confirmed in a dynamic structure because regulatory Cys residues of target proteins are mostly located on the flexible loops (42). Indeed, our results certainly show that the key residues for Trx-*f* interact with FBPase along with conformational changes (Movies S1–S3). Hence, such a dynamic structure or solution structure might be necessary to explore residues in both Trx and target that involved in their interaction. Although residues Asn-127 and Glu-156 could not make contact with the target protein molecule in our model within the calculation period, the distance between these residues and the target protein molecule was also continuously changing (Fig. 4*B*), implying that these residues may interact with the target protein during longer time-scale simulations.

The key residues for Trx-*f* are almost completely conserved among *f*-type Trxs in vascular plants (Fig. 10). This fact indicates that the target recognition mechanism of Trx-*f* is broadly conserved among vascular plants. Moreover, key residues for Trx-*f* are also conserved in moss and green algae Trx-*f* proteins, excluding one of the Trx-*f* isoforms of green algae (Fig. 10), whereas their mature protein sequence identity against *A. thaliana* Trx-*f*1 ranged from 40 to 67%. Trx-*f* from *Physcomitrella patens* lacks two of the key residues for Trx-*f*. This fact is in line with the previous result that *P. patens* Trx-*f* could reduce CROST1, but the efficiency was lower than that of *A. thaliana* Trx-*f*1 (31). We also compared amino acid sequences of Trx-*f* and NTRC, and we found that NTRC proteins have only a few residues of the key residues identified on Trx-*f* (Fig. 9*C*). Supportive of this alignment, NTRC has no reduction activity or very low reduction activity against Trx-*f*–specific targets *in vitro* (44), whereas NTRC is suggested to be (directly and/or indirectly) involved in reduction of these targets *in vivo* (19).

From the results of experiments ii and iii, we could validate the significance of the key residues on Trx-*f* for target recognition (Fig. 5). Together with the result of experiment i, our study revealed a hierarchy of the impact of the residues involved in the selectivity. In these key residues, the portion including α-helix 3 appeared to be most important for determining selectivity (see Trx-$m2_{f135-143}$ mutant in Fig. 5, *B* and *C*). It must be noted that even the combination of all of the feasible mutations (*f*135–172) could not increase the reduction activity of Trx-*m*2 to the same level as that of Trx-*f*1 (Fig. 5, *B* and *C*). Residues of Trx-*f*1, such as Met-94 and Thr-96, could have a certain role in this process, although we could not prepare mutants at these positions because of the insolubility of recombinant proteins. Another candidate residue involved in the interaction is Asn-130. We did not include this residue as a potential key residue for Trx-*f* because a previous study revealed that the ambiguous assignment of this residue is Trx-*f*–specific depending on the alignment (24). Nevertheless, the apparent capacities of Trx-*m*2 mutants, ACHT1 and ACHT2a, to reduce Trx-*f*–

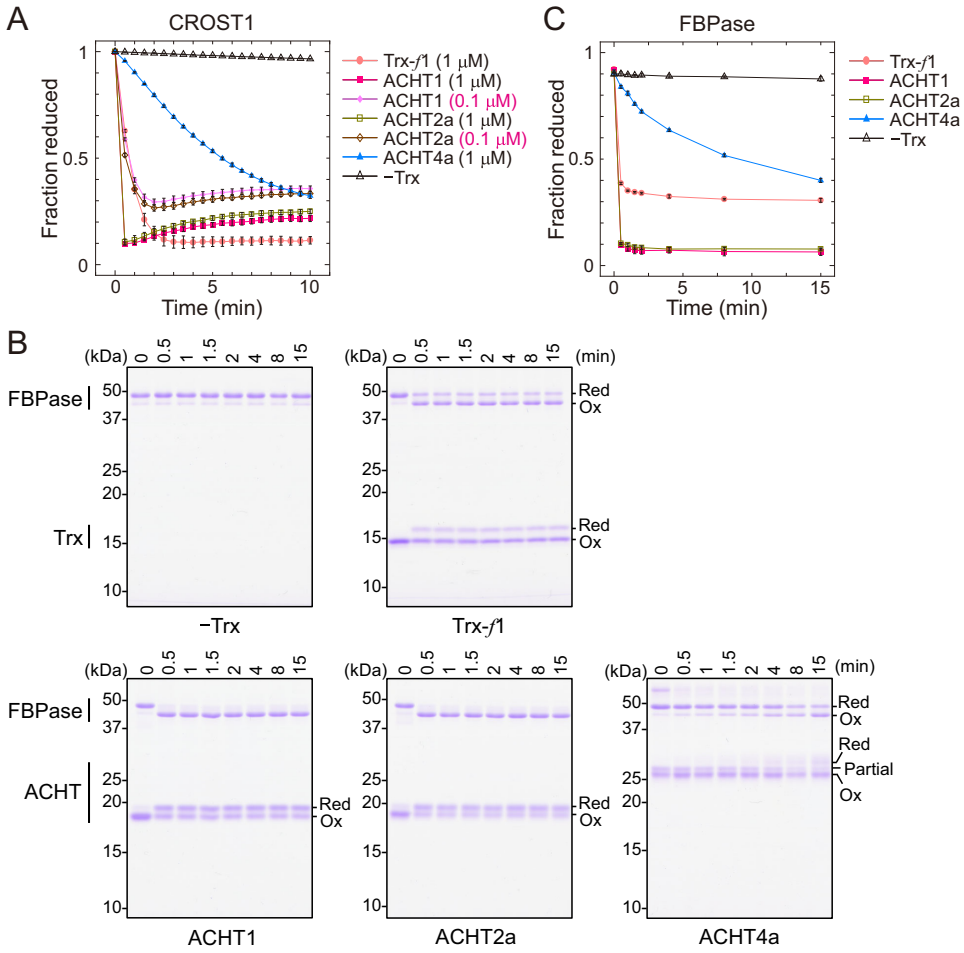

Figure 7. Capacity of ACHTs to oxidize Trx-*f*–specific targets. *A,* time-dependent oxidation of CROST1 by Trx-*f*1 and ACHT proteins. In the presence of 50 mM oxidized DTT, 0.1 μM reduced CROST1 was incubated with 1 μM Trx, 1 μM ACHT, 0.1 μM ACHT1, or 0.1 μM ACHT2a, and the redox state of CROST1 was monitored by measuring the FRET intensity. Each value represents the mean ± S.D. ($n = 3$). *B,* determination of the redox state of FBPase oxidized by Trx-*f*1 and ACHT proteins. Without the oxidizing reagent, 2 μM reduced FBPase was incubated with 2 μM oxidized Trx or ACHT and precipitated at each time point. Reduced (*Red*) and oxidized (*Ox*) proteins were discriminated via the thiol group modification using 4-acetamido-4′-maleimidylstilbene-2,2′-disulfonate followed by SDS-PAGE. *C,* time-dependent oxidation of FBPase by Trx-*f*1 and ACHT proteins. Redox state of FBPase was determined in *B* and plotted. Each value represents the mean ± S.D. ($n = 3$).

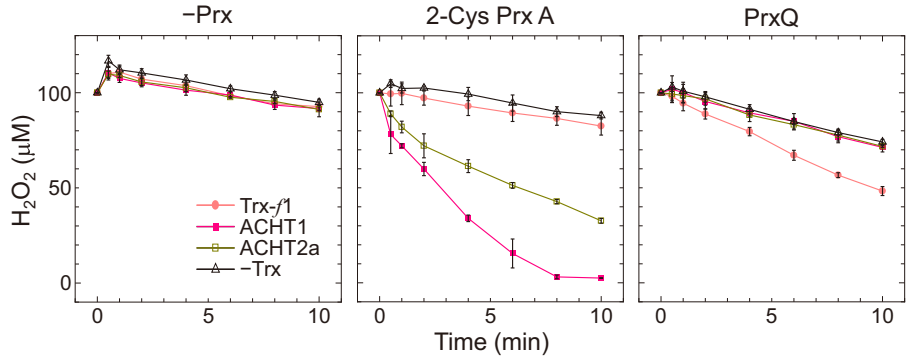

Figure 8. Trx- or ACHT-dependent H_2O_2 detoxification by Prxs. H_2O_2 detoxification by Prxs with 0.5 mM reduced DTT in the presence or absence of Trx-*f*1 or ACHT was monitored as described under "Experimental procedures." Each value represents the mean ± S.D. ($n = 3$).

specific targets indicate that the key residues identified on Trx-*f* are the major determinants of their target selectivity.

On the oxidation process

As mentioned previously, one of the determinants of the rate and direction of redox reaction is the E_m values of the electron donor and acceptor, although their physical interaction is certainly a prerequisite for the reaction. Because ACHT1 and ACHT2a could efficiently perform the dithiol–disulfide exchange reaction with Trx-*f*–specific targets (Fig. 5, *B* and *E*), we determined their E_m values, and they were remarkably high similar to those of TrxL2 proteins (Fig. 6). Because the amino

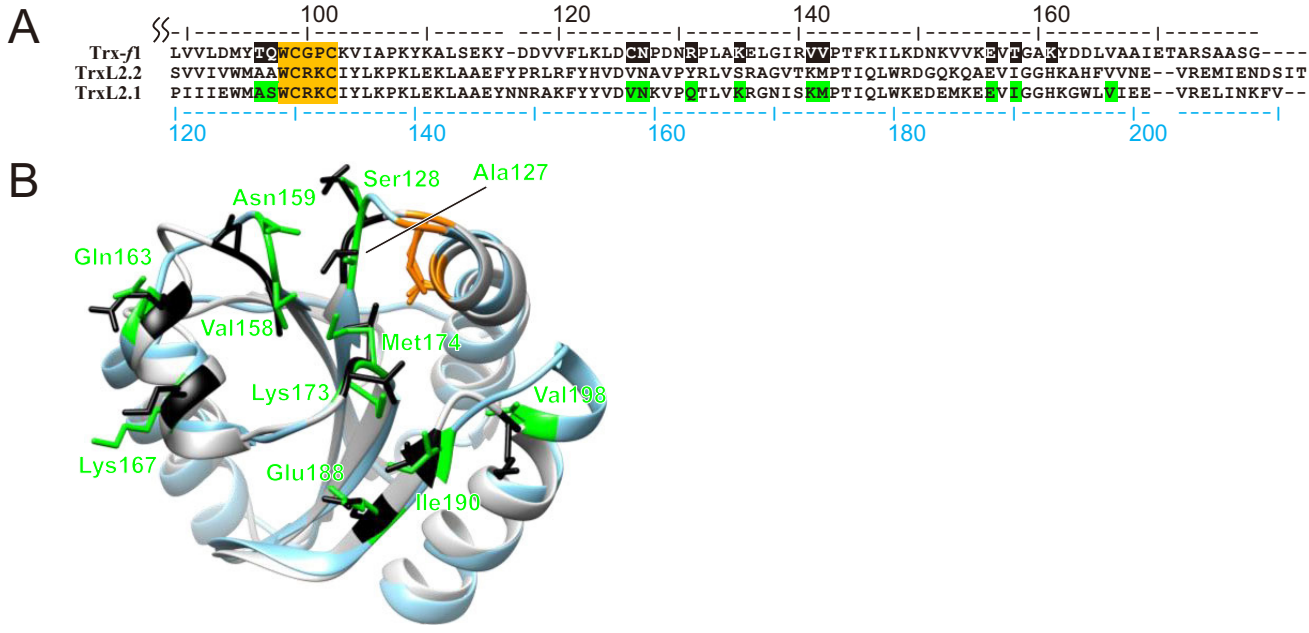

Figure 9. Conservation of the key residues for Trx-*f* in TrxL2 and NTRC molecules. *A,* amino acid sequence comparison of Trx-*f*1 and TrxL2 proteins. The residue numbers of Trx-*f*1 and TrxL2.1 counted from the translational start site amino acid methionine are indicated *above* (*black*) and *below* (*sky blue*) the alignment result, respectively. *B,* structure comparison of Trx-*f*1 (*light gray*) and TrxL2.1 (*sky blue*). *A* and *B,* residues of TrxL2.1 corresponding to the key residues for Trx-*f* are highlighted in *green*. *C,* amino acid sequence comparison of Trx-*f*1 and Trx domains of plant NTRCs. The residue numbers of *A. thaliana* NTRC counted from the translational start site amino acid methionine are shown *above the figure*. Residues highlighted in *magenta* are the *cis*-Pro−1 residues of NTRC. Full names of the organisms are described in Table S1. *A–C,* residues highlighted in *orange* and *black* are the active site and the key residues for Trx-*f*, respectively.

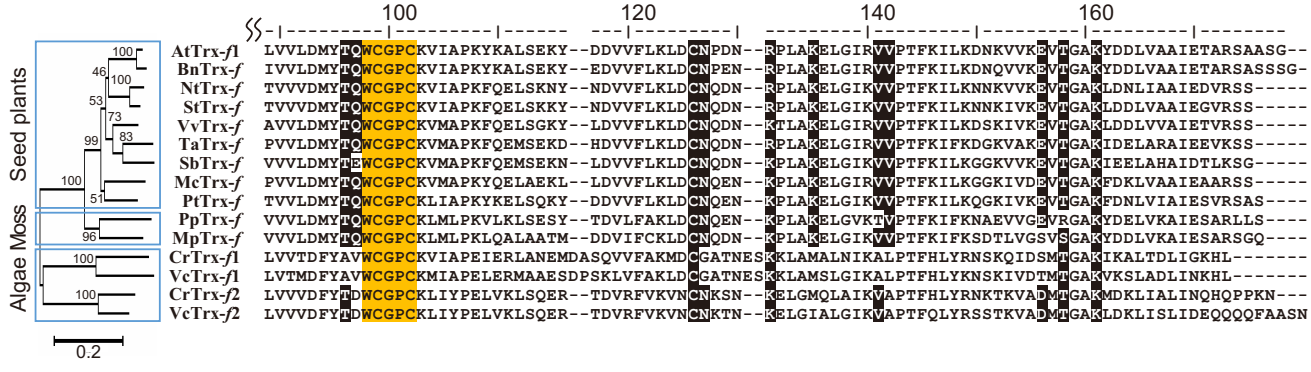

Figure 10. Conservation of the key residues for Trx-*f* among Trx-*f* proteins from various plants. The residue numbers of *A. thaliana* Trx-*f*1 (counted from the translational start site amino acid methionine) are shown *above the figure*. Residues highlighted in *orange* and *black* are the active site and the key residues for Trx-*f*, respectively. The phylogenetic tree is shown with bootstrap values (%). Full names of the organisms are described in Table S1.

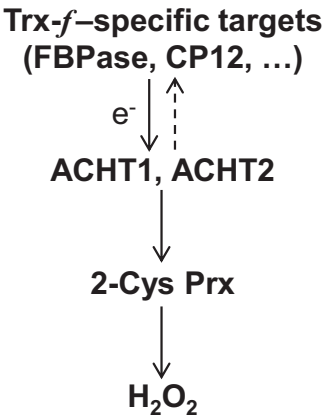

Figure 11. Redox cascade proposed in this study. *Arrows* indicate electron transfer reactions. *Dashed line arrow* indicates less efficient reaction.

acid residues around active-site cysteines and the *cis*-Pro−1 residue influence the E_m value of Trx (20, 45–47), these residues might increase the E_m values of ACHT1 and ACHT2a as well. We therefore examined whether ACHT1 and ACHT2a can also oxidize Trx-*f*–specific targets. As shown in Fig. 7, they could oxidize both CROST1 and FBPase more efficiently than Trx-*f*1. The efficiency was also higher than that of ACHT4a (Fig. 7) and TrxL2 proteins (refer our previous results shown in Refs. 31, 32), probably because only the part of the key residues for Trx-*f* are conserved in ACHT4a and TrxL2 compared with the sequences of ACHT1 and ACHT2a (Figs. 5*D*, and 9, *A* and *B*). Because ACHT1 and ACHT2a lack several key residues, it is possible that introduction of these residues to ACHT1 or ACHT2a increases their reduction and oxidation activities.

As discussed previously, ACHT1 and ACHT2a can receive reducing power from their targets. We therefore investigated the acceptor of the reducing power and found that they can efficiently transfer reducing power to 2-Cys PrxA and finally to H_2O_2 (Fig. 8), similarly as TrxL2 proteins (32, 48). The interaction between ACHT proteins and 2-Cys Prx *in vivo* and *in vitro* has already been reported (33, 48–50), suggesting that 2-Cys Prx is also an efficient electron acceptor for ACHT proteins, although these previous studies did not present direct evidence of target oxidation by ACHT1 or ACHT2a. In addition, the most recent studies indicated that 2-Cys Prx is the major acceptor of the reducing power of Trx–targeted proteins in chloroplasts (32, 51–53). Although the major reductant of 2-Cys Prx is NTRC, a part of oxidizing power via 2-Cys Prx might be used for the oxidation of redox-regulated proteins via oxidation factors *in vivo*. Our results in this study, together with these previous findings, strongly suggest that ACHT1 and ACHT2a are efficient oxidation factors at least for Trx-*f*–specific target proteins, and they ultimately transfer reducing power to H_2O_2 via 2-Cys Prx (Fig. 11).

In this study, we identified the key residues for Trx-*f*–specific target recognition. In addition, we successfully uncovered the roles of ACHT1 and ACHT2a as oxidation factors. Our results imply the existence of target selectivity in the oxidative regulation of photosynthesis, and this selectivity can be inferred from the information on the target selectivity of typical Trxs and amino acid sequences of Trx-like proteins.

Experimental procedures

In silico analyses

The amino acid sequences presented in this study were obtained from the UniProtKB database (https://www.uniprot.org/)[3] and the Arabidopsis Information Resource database. Their accession numbers are listed in Table S1.

Multiple sequence alignment was performed using the Clustal Omega program (https://www.ebi.ac.uk/)[3] with default parameters. Using the result of the multiple sequence alignment and MEGA7 software (54), phylogenetic relationships were inferred via the neighbor-joining method with 500 bootstrap replicates.

Residues involved in Trx–target or Trx-TrxR interactions were predicted using the Protein Interaction Calculator web server (55) with default parameters and various structures (PDB codes: 1SKR, 2IPA, 2IWT, 2O8V, 3PIN, 4DSS, 4LL1, 1CQG, 2PU9, 2PUK, 1F6M, 3QFA, and 4J56).

Models of the three-dimensional structures of AtTrx-*f*1 and TrxL2.1 were built using the SWISS-MODEL program (https://swissmodel.expasy.org/) (56) with their amino acid sequences and the structures of SoTrx-*f* (PDB code 1F9M) and poplar TrxL2.1 (PDB code 5NYK) as templates. The ribbon structure and molecular surface of the models were visualized using UCSF Chimera software (57).

Modeling

To construct an atomic model of the complex structure of Trx-*f* and FBPase, first we performed a protein–protein docking calculation between spinach Trx-*f* (1F9M.pdb (58)) and pea FBPase (1D9Q.pdb (59)) using rigid-body docking ZDOCK 3.0.2 (60, 61). The dense mode (grid search of the rotational space at 6° increments) was used, and the docking procedure was repeated 10 times to generate 540,000 complex models. Among them, optimum models were chosen whose distances between the Cys residues of Trx-*f* (Cys-46 and Cys-49) and those of FBPase (Cys-153 and Cys-173) are the closest. Three models were selected based on the sulfur–sulfur distances of the Cys residues in the two proteins. To conduct structure refinement of these models, 500-ns MD simulation was performed for each model. MD simulations were performed using Gromacs 2018.1 (62, 63). The system was brought to thermodynamic equilibrium at 300 K and 1 atm using the Nosé-Hoover thermostat and the Parrinello-Rahman barostat. The equations of motion were integrated with a time step of 2 fs. Long-range Coulomb energy was evaluated using the particle mesh Ewald (PME) method. The ff14SB force field (64) and SPC/Eb model (65) were used for protein and water models, respectively. The best model was selected based on the sulfur–sulfur distances obtained from MD simulations. Employing a representing structure of the spinach Trx-*f*/pea FBPase complex as a template, we next constructed an atomic model structure of the *A. thaliana* Trx-*f*1/FBPase complex. The structure used for the homology modeling was the representative structure of the dominant cluster obtained by clustering the MD trajectory, and

[3] Please note that the JBC is not responsible for the long-term archiving and maintenance of this site or any other third party hosted site.

the homology modeling was conducted with the SWISS-MODEL server (56). Finally, we performed 300-ns MD simulations of the obtained model structure in explicit water to refine the structure and analyzed inter-molecular interactions.

Preparation of expression plasmids

All proteins used in this study, excluding CROST1, were derived from *A. thaliana*. Total RNA was extracted from frozen *Arabidopsis* leaves using the TRIzol reagent (Invitrogen) according to the manufacturer's instructions. cDNA was synthesized via RT-PCR with extracted RNA and was used for expression plasmid construction.

Mature protein-coding regions of ACHT1, ACHT2a, and ACHT4a described in previous research (48) were cloned into the pET-23c vector (Novagen) to express C-terminally His-tagged recombinant proteins. Expression plasmids for Trx-*f*1, Trx-*m*2, PrxQ, 2-Cys PrxA, and CROST1 were constructed previously (18, 31, 44). For FBPase expression, the previously constructed plasmid (18) was modified to enhance its expression in *E. coli* via site-directed mutagenesis in accordance with the 31C-FO_H method described by Boël *et al.* (66). To express Trx-*f*1 mutants and Trx-*m*2 mutants, mutations were introduced into each expression plasmid via site-directed mutagenesis. Site-directed mutagenesis was performed using a PrimeSTAR mutagenesis basal kit (Takara) according to the manufacturer's instructions. The primers used for cloning and site-directed mutagenesis are shown in Table S2.

Protein expression and purification

E. coli strain BL21(DE3) pLysS (for Trxs and FBPase) or strain BL21(DE3) (for ACHTs, CROST1, and Prxs) was transformed with each expression plasmid. Transformed cells were cultured at 37 °C, and expression was subsequently induced by adding isopropyl β-D-thiogalactopyranoside (final concentration, 0.5 mM) followed by further culture for 16 h at 21 °C. Collected cells were disrupted and centrifuged (125,000 × *g* for 40 min) to obtain the soluble fraction containing the protein of interest for subsequent purification. CROST1 was purified as described previously (31). Trxs and ACHTs were purified via a combination of nickel-nitrilotriacetic acid affinity chromatography with nickel-nitrilotriacetic acid–agarose (Qiagen), cation-exchange chromatography (CEC) with TOYOPEARL SP-650 M (Tosoh) (this step was only for ACHTs), and size-exclusion chromatography (SEC) with Superdex 75 Increase 10/300 GL (GE Healthcare). The other proteins were purified via anion-exchange chromatography with TOYOPEARL DEAE-650 M (Tosoh) (for FBPase and 2-Cys PrxA) or CEC with TOYOPEARL SP-650 M (for PrxQ), followed by hydrophobic-interaction chromatography (HIC) with TOYOPEARL Butyl-650 M (Tosoh). Trxs, and ACHTs were treated with 2 mM reduced DTT for 15 min before SEC. FBPase and Prxs were treated with 1 mM diamide and 0.5 mM H_2O_2, respectively, for 1 h after HIC. Finally, medium containing each protein was replaced by buffer containing 25 mM Tris-HCl (pH 7.5) and 150 mM NaCl (for Trxs); 25 mM Tris-HCl (pH 7.5), 150 mM NaCl, and 50 μM EDTA (for ACHTs); or 25 mM Tris-HCl (pH 7.5) (for the others) during SEC; alternatively, dialysis was performed after HIC. All purification steps were performed at 4 °C. The concentrations of the purified proteins were determined using a BCA protein assay kit (Pierce).

Insulin reduction assay

The capacity of Trx to reduce disulfide bonds was determined via an insulin reduction assay according to previous studies with minor modifications (18, 36). The reaction was initiated by adding reduced DTT (final concentration, 0.5 mM) into a reaction mixture containing 50 mM Tris-HCl (pH 7.5), 50 mM NaCl, 1 mM EDTA, 230 μM bovine insulin (Sigma), and 5 μM Trx. Turbidity, which resulted from reduced insulin, was monitored at 650 nm at 25 °C. Insulin reduction activity ($\Delta OD_{650\ nm}\ min^{-1}$) was determined via linear regression of the data, for which $OD_{650\ nm}$ ranged from 0.2 to 0.8.

Target reduction and oxidation assays

For the target reduction and oxidation assays, medium containing 1 mM EDTA (only for CROST1), 50 mM Tris-HCl (pH 7.5), and 50 mM NaCl was used, and the reaction was performed at 25 °C. The redox states of CROST1 and FBPase were monitored via the emission of fluorescence at 480 and 530 nm, and the thiol group modification-based method, as described previously (18, 31). For the target oxidation assay, targets were reduced before the assay as described previously (31, 32). For the FBPase oxidation assay, 0.6 μM Trx-*f*1 or ACHT was pre-incubated in medium containing 25 mM Tris-HCl (pH 7.5), 50 mM oxidized DTT, and 1 μM reduced DTT for 3 h at 25 °C, and DTT was then removed via SEC. The concentrations of proteins and DTT used for each reaction are shown in each figure legend. Target reduction activities were calculated by fitting the data of the time-dependent reduction assay to Equation 1 built in accordance with a previous study (31),

$$[target_{red}]/[target_{total}] = 1 - e^{-k[Trx]_t} \quad \text{(Eq. 1)}$$

where k ($\mu M^{-1}\ min^{-1}$) is the rate constant used to determine the activity of Trx, and t (min) is time after the reaction was initiated.

Determination of E_m

E_m values of Trx-*f*1 mutants are roughly estimated as described under "Results." E_m values of ACHT proteins were determined essentially as described previously (18). ACHT (0.6 μM) was incubated for 3 h at 25 °C in medium containing 25 mM Tris-HCl (pH 7.5), 50 mM oxidized DTT, and 0.0005–5 mM reduced DTT. After the incubation, the ratio of oxidized and reduced form at each redox potential was determined via the thiol group modification-based method. E_m values of ACHT proteins were calculated by fitting the obtained data to the Nernst equation. The redox potential of each reaction mixture was calculated using −357 mV as E_m of DTT at pH 7.5.

H_2O_2 detoxification assay

To monitor the reduction of Prxs by Trx-*f*1 or ACHT, 2 μM 2-Cys PrxA or PrxQ was incubated with 1 μM Trx or ACHT in medium containing 50 mM Tris-HCl (pH 7.5), 50 mM NaCl, 0.5 mM reduced DTT, and 100 μM H_2O_2 at 25 °C. At each indicated time, the H_2O_2 concentration in the reaction mixture was

determined via ferrous oxidation in the xylenol orange assay (67).

Author contributions—Y. Y., K. S., K. Y., and T. H. conceptualization; Y. Y., K. S., K. T., K. Y., and S. H. investigation; Y. Y. and T. H. writing-original draft; K. Y., K. W., A. K., and T. H. writing-review and editing; K. W., A. K., and T. H. supervision.

Acknowledgments—We thank the Biomaterials Analysis Division, Tokyo Institute of Technology, for supporting DNA sequencing analysis, and the Suzukakedai Materials Analysis Division, Tokyo Institute of Technology, for supporting MS analysis. The computations were partly performed using the supercomputers at the RCCS, National Institute of Natural Science, and ISSP, University of Tokyo. This research also used computational resources of the K computer provided by the RIKEN Advanced Institute for Computational Science through the HPCI System Research Project IDs hp150270, hp160207, hp170254, hp180201, and hp190181.

References

1. Martin, J. L. (1995) Thioredoxin–a fold for all reasons. *Structure* **3,** 245–250 CrossRef Medline
2. Collet, J. F., and Messens, J. (2010) Structure, function, and mechanism of thioredoxin proteins. *Antioxid. Redox Signal.* **13,** 1205–1216 CrossRef Medline
3. Ingles-Prieto, A., Ibarra-Molero, B., Delgado-Delgado, A., Perez-Jimenez, R., Fernandez, J. M., Gaucher, E. A., Sanchez-Ruiz, J. M., and Gavira, J. A. (2013) Conservation of protein structure over four billion years. *Structure* **21,** 1690–1697 CrossRef Medline
4. Buchanan, B. B. (1980) Role of light in the regulation of chloroplast enzymes. *Annu. Rev. Plant Physiol. Plant Mol. Biol.* **31,** 341–374 CrossRef
5. Jacquot, J.-P., Vidal, J., Gadal, P., and Schürmann, P. (1978) Evidence for the existence of several enzyme-specific thioredoxins in plants. *FEBS Lett.* **96,** 243–246 CrossRef
6. Wolosiuk, R. A., Crawford, N. A., Yee, B. C., and Buchanan, B. B. (1979) Isolation of three thioredoxins from spinach leaves. *J. Biol. Chem.* **254,** 1627–1632 Medline
7. Schurmann, P., Maeda, K., and Tsugita, A. (1981) Isomers in thioredoxins of spinach chloroplasts. *Eur. J. Biochem.* **116,** 37–45 Medline
8. Michelet, L., Zaffagnini, M., Morisse, S., Sparla, F., Pérez-Pérez, M. E., Francia, F., Danon, A., Marchand, C. H., Fermani, S., Trost, P., and Lemaire, S. D. (2013) Redox regulation of the Calvin-Benson cycle: something old, something new. *Front. Plant Sci.* **4,** 470 CrossRef
9. Wenderoth, I., Scheibe, R., and von Schaewen, A. (1997) Identification of the cysteine residues involved in redox modification of plant plastidic glucose-6-phosphate dehydrogenase. *J. Biol. Chem.* **272,** 26985–26990 CrossRef Medline
10. Mills, J. D., Mitchell, P., and Schurmann, P. (1980) Modulation of coupling factor ATPase activity in intact chloroplasts, the role of the thioredoxin system. *FEBS Lett.* **112,** 173–177 CrossRef
11. Arabidopsis Genome Initiative. (2000) Analysis of the genome sequence of the flowering plant *Arabidopsis thaliana*. *Nature* **408,** 796–815 CrossRef Medline
12. Yano, H., Wong, J. H., Lee, Y. M., Cho, M. J., and Buchanan, B. B. (2001) A strategy for the identification of proteins targeted by thioredoxin. *Proc. Natl. Acad. Sci. U.S.A.* **98,** 4794–4799 CrossRef Medline
13. Motohashi, K., Kondoh, A., Stumpp, M. T., and Hisabori, T. (2001) Comprehensive survey of proteins targeted by chloroplast thioredoxin. *Proc. Natl. Acad. Sci. U.S.A.* **98,** 11224–11229 CrossRef Medline
14. Lindahl, M., and Kieselbach, T. (2009) Disulphide proteomes and interactions with thioredoxin on the track towards understanding redox regulation in chloroplasts and cyanobacteria. *J. Proteomics* **72,** 416–438 CrossRef Medline
15. Montrichard, F., Alkhalfioui, F., Yano, H., Vensel, W. H., Hurkman, W. J., and Buchanan, B. B. (2009) Thioredoxin targets in plants: the first 30 years. *J. Proteomics* **72,** 452–474 CrossRef Medline
16. Collin, V., Issakidis-Bourguet, E., Marchand, C., Hirasawa, M., Lancelin, J. M., Knaff, D. B., and Miginiac-Maslow, M. (2003) The *Arabidopsis* plastidial thioredoxins: new functions and new insights into specificity. *J. Biol. Chem.* **278,** 23747–23752 CrossRef Medline
17. Marri, L., Zaffagnini, M., Collin, V., Issakidis-Bourguet, E., Lemaire, S. D., Pupillo, P., Sparla, F., Miginiac-Maslow, M., and Trost, P. (2009) Prompt and easy activation by specific thioredoxins of calvin cycle enzymes of *Arabidopsis thaliana* associated in the GAPDH/CP12/PRK supramolecular complex. *Mol. Plant* **2,** 259–269 CrossRef Medline
18. Yoshida, K., Hara, S., and Hisabori, T. (2015) Thioredoxin selectivity for thiol-based redox regulation of target proteins in chloroplasts. *J. Biol. Chem.* **290,** 19540 CrossRef Medline
19. Geigenberger, P., Thormählen, I., Daloso, D. M., and Fernie, A. R. (2017) The unprecedented versatility of the plant thioredoxin system. *Trends Plant Sci.* **22,** 249–262 CrossRef Medline
20. Ren, G., Stephan, D., Xu, Z., Zheng, Y., Tang, D., Harrison, R. S., Kurz, M., Jarrott, R., Shouldice, S. R., Hiniker, A., Martin, J. L., Heras, B., and Bardwell, J. C. (2009) Properties of the thioredoxin fold superfamily are modulated by a single amino acid residue. *J. Biol. Chem.* **284,** 10150–10159 CrossRef Medline
21. Yoshida, K., and Hisabori, T. (2017) Distinct electron transfer from ferredoxin-thioredoxin reductase to multiple thioredoxin isoforms in chloroplasts. *Biochem. J.* **474,** 1347–1360 CrossRef Medline
22. Hirasawa, M., Schürmann, P., Jacquot, J. P., Manieri, W., Jacquot, P., Keryer, E., Hartman, F. C., and Knaff, D. B. (1999) Oxidation–reduction properties of chloroplast thioredoxins, ferredoxin:thioredoxin reductase, and thioredoxin f-regulated enzymes. *Biochemistry* **38,** 5200–5205 CrossRef Medline
23. Yoshida, K., and Hisabori, T. (2018) Determining the rate-limiting step for light-responsive redox regulation in chloroplasts. *Antioxidants* **7,** E153 CrossRef Medline
24. de Lamotte-Guery, F., Miginiac-Maslow, M., Decottignies, P., Stein, M., Minard, P., and Jacquot, J. P. (1991) Mutation of a negatively charged amino acid in thioredoxin modifies its reactivity with chloroplastic enzymes. *Eur. J. Biochem.* **196,** 287–294 CrossRef Medline
25. Geck, M. K., Larimer, F. W., and Hartman, F. C. (1996) Identification of residues of spinach thioredoxin f that influence interactions with target enzymes. *J. Biol. Chem.* **271,** 24736–24740 CrossRef Medline
26. Mora-García, S., Rodríguez-Suárez, R., and Wolosiuk, R. A. (1998) Role of electrostatic interactions on the affinity of thioredoxin for target proteins. Recognition of chloroplast fructose-1,6-bisphosphatase by mutant *Escherichia coli* thioredoxins. *J. Biol. Chem.* **273,** 16273–16280 CrossRef Medline
27. Geck, M. K., and Hartman, F. C. (2000) Kinetic and mutational analyses of the regulation of phosphoribulokinase by thioredoxins. *J. Biol. Chem.* **275,** 18034–18039 CrossRef Medline
28. Wangensteen, O. S., Chueca, A., Hirasawa, M., Sahrawy, M., Knaff, D. B., and López Gorgé, J. (2001) Binding features of chloroplast fructose-1,6-bisphosphatase–thioredoxin interaction. *Biochim. Biophys. Acta* **1547,** 156–166 CrossRef Medline
29. Collin, V., Lamkemeyer, P., Miginiac-Maslow, M., Hirasawa, M., Knaff, D. B., Dietz, K. J., and Issakidis-Bourguet, E. (2004) Characterization of plastidial thioredoxins from *Arabidopsis* belonging to the new y-type. *Plant Physiol.* **136,** 4088–4095 CrossRef Medline
30. Arsova, B., Hoja, U., Wimmelbacher, M., Greiner, E., Ustün, S., Melzer, M., Petersen, K., Lein, W., and Börnke, F. (2010) Plastidial thioredoxin z interacts with two fructokinase-like proteins in a thiol-dependent manner: evidence for an essential role in chloroplast development in *Arabidopsis* and *Nicotiana benthamiana*. *Plant Cell* **22,** 1498–1515 CrossRef Medline
31. Sugiura, K., Yokochi, Y., Fu, N., Fukaya, Y., Yoshida, K., Mihara, S., Fu, N., and Hisabori, T. (2019) The thioredoxin (Trx) redox-state sensor protein can visualize Trx activities in the light-dark response in chloroplasts. *J. Biol. Chem.* **294,** 12091–12098 CrossRef Medline

32. Yoshida, K., Hara, A., Sugiura, K., Fukaya, Y., and Hisabori, T. (2018) Thioredoxin-like2/2-Cys peroxiredoxin redox cascade supports oxidative thiol modulation in chloroplasts. *Proc. Natl. Acad. Sci. U.S.A.* **115,** E8296–E8304 CrossRef Medline
33. Eliyahu, E., Rog, I., Inbal, D., and Danon, A. (2015) ACHT4-driven oxidation of APS1 attenuates starch synthesis under low light intensity in *Arabidopsis* plants. *Proc. Natl. Acad. Sci. U.S.A.* **112,** 12876–12881 CrossRef Medline
34. Meyer, Y., Reichheld, J. P., and Vignols, F. (2005) Thioredoxins in *Arabidopsis* and other plants. *Photosynth. Res.* **86,** 419–433 CrossRef Medline
35. Chibani, K., Wingsle, G., Jacquot, J. P., Gelhaye, E., and Rouhier, N. (2009) Comparative genomic study of the thioredoxin family in photosynthetic organisms with emphasis on *Populus trichocarpa*. *Mol. Plant* **2,** 308–322 CrossRef Medline
36. Holmgren, A. (1979) Thioredoxin catalyzes the reduction of insulin disulfides by dithiothreitol and dihydrolipoamide. *J. Biol. Chem.* **254,** 9627–9632 Medline
37. Vanacker, H., Guichard, M., Bohrer, A. S., and Issakidis-Bourguet, E. (2018) Redox regulation of monodehydroascorbate reductase by thioredoxin y in plastids revealed in the context of water stress. *Antioxidants* **7,** E183 CrossRef Medline
38. Schröter, Y., Steiner, S., Matthäi, K., and Pfannschmidt, T. (2010) Analysis of oligomeric protein complexes in the chloroplast sub-proteome of nucleic acid-binding proteins from mustard reveals potential redox regulators of plastid gene expression. *Proteomics* **10,** 2191–2204 CrossRef Medline
39. Steiner, S., Schröter, Y., Pfalz, J., and Pfannschmidt, T. (2011) Identification of essential subunits in the plastid-encoded RNA polymerase complex reveals building blocks for proper plastid development. *Plant Physiol.* **157,** 1043–1055 CrossRef Medline
40. Wimmelbacher, M., and Börnke, F. (2014) Redox activity of thioredoxin z and fructokinase-like protein 1 is dispensable for autotrophic growth of *Arabidopsis thaliana*. *J. Exp. Bot.* **65,** 2405–2413 CrossRef Medline
41. Díaz, M. G., Hernández-Verdeja, T., Kremnev, D., Crawford, T., Dubreuil, C., and Strand, Å. (2018) Redox regulation of PEP activity during seedling establishment in *Arabidopsis thaliana*. *Nat. Commun.* **9,** 50 CrossRef Medline
42. Gütle, D. D., Roret, T., Hecker, A., Reski, R., and Jacquot, J. P. (2017) Dithiol disulphide exchange in redox regulation of chloroplast enzymes in response to evolutionary and structural constraints. *Plant Sci.* **255,** 1–11 CrossRef Medline
43. Lemaire, S. D., Tedesco, D., Crozet, P., Michelet, L., Fermani, S., Zaffagnini, M., and Henri, J. (2018) Crystal structure of chloroplastic thioredoxin f2 from *Chlamydomonas reinhardtii* reveals distinct surface properties. *Antioxidants* **7,** E171 CrossRef Medline
44. Yoshida, K., and Hisabori, T. (2016) Two distinct redox cascades cooperatively regulate chloroplast functions and sustain plant viability. *Proc. Natl. Acad. Sci. U.S.A.* **113,** E3967–E3976 CrossRef Medline
45. Dyson, H. J., Gippert, G. P., Case, D. A., Holmgren, A., and Wright, P. E. (1990) Three-dimensional solution structure of the reduced form of *Escherichia coli* thioredoxin determined by nuclear magnetic resonance spectroscopy. *Biochemistry* **29,** 4129–4136 CrossRef Medline
46. Lundström, J., Krause, G., and Holmgren, A. (1992) A Pro to His mutation in active site of thioredoxin increases its disulfide-isomerase activity 10-fold. New refolding systems for reduced or randomly oxidized ribonuclease. *J. Biol. Chem.* **267,** 9047–9052 Medline
47. Chibani, K., Tarrago, L., Gualberto, J. M., Wingsle, G., Rey, P., Jacquot, J. P., and Rouhier, N. (2012) Atypical thioredoxins in poplar: the glutathione-dependent thioredoxin-like 2.1 supports the activity of target enzymes possessing a single redox active cysteine. *Plant Physiol.* **159,** 592–605 CrossRef Medline
48. Dangoor, I., Peled-Zehavi, H., Levitan, A., Pasand, O., and Danon, A. (2009) A small family of chloroplast atypical thioredoxins. *Plant Physiol.* **149,** 1240–1250 CrossRef Medline
49. Dangoor, I., Peled-Zehavi, H., Wittenberg, G., and Danon, A. (2012) A chloroplast light-regulated oxidative sensor for moderate light intensity in *Arabidopsis*. *Plant Cell* **24,** 1894–1906 CrossRef Medline
50. Cerveau, D., Kraut, A., Stotz, H. U., Mueller, M. J., Couté, Y., and Rey, P. (2016) Characterization of the *Arabidopsis thaliana* 2-Cys peroxiredoxin interactome. *Plant Sci.* **252,** 30–41 CrossRef Medline
51. Pérez-Ruiz, J. M., Naranjo, B., Ojeda, V., Guinea, M., and Cejudo, F. J. (2017) NTRC-dependent redox balance of 2-Cys peroxiredoxins is needed for optimal function of the photosynthetic apparatus. *Proc. Natl. Acad. Sci. U.S.A.* **114,** 12069–12074 CrossRef Medline
52. Vaseghi, M. J., Chibani, K., Telman, W., Liebthal, M. F., Gerken, M., Schnitzer, H., Mueller, S. M., and Dietz, K. J. (2018) The chloroplast 2-cysteine peroxiredoxin functions as thioredoxin oxidase in redox regulation of chloroplast metabolism. *Elife* **7,** e38194 CrossRef Medline
53. Ojeda, V., Pérez-Ruiz, J. M., and Cejudo, F. J. (2018) 2-Cys peroxiredoxins participate in the oxidation of chloroplast enzymes in the dark. *Mol. Plant* **11,** 1377–1388 CrossRef Medline
54. Kumar, S., Stecher, G., and Tamura, K. (2016) MEGA7: molecular evolutionary genetics analysis version 7.0 for bigger datasets. *Mol. Biol. Evol.* **33,** 1870–1874 CrossRef Medline
55. Tina, K. G., Bhadra, R., and Srinivasan, N. (2007) PIC: protein interactions calculator. *Nucleic Acids Res.* **35,** W473–W476 CrossRef Medline
56. Waterhouse, A., Bertoni, M., Bienert, S., Studer, G., Tauriello, G., Gumienny, R., Heer, F. T., de Beer, T. A. P., Rempfer, C., Bordoli, L., Lepore, R., and Schwede, T. (2018) SWISS-MODEL: homology modelling of protein structures and complexes. *Nucleic Acids Res.* **46,** W296–W303 CrossRef Medline
57. Pettersen, E. F., Goddard, T. D., Huang, C. C., Couch, G. S., Greenblatt, D. M., Meng, E. C., and Ferrin, T. E. (2004) UCSF Chimera–a visualization system for exploratory research and analysis. *J. Comput. Chem.* **25,** 1605–1612 CrossRef Medline
58. Capitani, G., Marković-Housley, Z., DelVal, G., Morris, M., Jansonius, J. N., and Schürmann, P. (2000) Crystal structures of two functionally different thioredoxins in spinach chloroplasts. *J. Mol. Biol.* **302,** 135–154 CrossRef Medline
59. Chiadmi, M., Navaza, A., Miginiac-Maslow, M., Jacquot, J. P., and Cherfils, J. (1999) Redox signalling in the chloroplast: structure of oxidized pea fructose-1,6-bisphosphate phosphatase. *EMBO J.* **18,** 6809–6815 CrossRef Medline
60. Chen, R., and Weng, Z. (2002) Docking unbound proteins using shape complementarity, desolvation, and electrostatics. *Proteins* **47,** 281–294 CrossRef Medline
61. Pierce, B. G., Hourai, Y., and Weng, Z. (2011) Accelerating protein docking in ZDOCK using an advanced 3D convolution library. *PLoS One* **6,** e24657 CrossRef Medline
62. Abraham, M. J., Murtola, T., Schulz, R., Páll, S., Smith, J. C., Hess, B., and Lindahl, E. (2015) GROMACS: high performance molecular simulations through multi-level parallelism from laptops to supercomputers. *SoftwareX* **1,** 19–25 CrossRef
63. Berendsen, H. J. C., van der Spoel, D., and van Drunen, R. (1995) GROMACS: a message-passing parallel molecular dynamics implementation. *Comput. Phys. Commun.* **91,** 43–56 CrossRef
64. Maier, J. A., Martinez, C., Kasavajhala, K., Wickstrom, L., Hauser, K. E., and Simmerling, C. (2015) ff14SB: improving the accuracy of protein side chain and backbone parameters from ff99SB. *J. Chem. Theory Comput.* **11,** 3696–3713 CrossRef Medline
65. Takemura, K., and Kitao, A. (2012) Water model tuning for improved reproduction of rotational diffusion and NMR spectral density. *J. Phys. Chem. B* **116,** 6279–6287 CrossRef Medline
66. Boël, G., Letso, R., Neely, H., Price, W. N., Wong, K. H., Su, M., Luff, J., Valecha, M., Everett, J. K., Acton, T. B., Xiao, R., Montelione, G. T., Aalberts, D. P., and Hunt, J. F. (2016) Codon influence on protein expression in *E. coli* correlates with mRNA levels. *Nature* **529,** 358–363 CrossRef Medline
67. Wolff, S. P. (1994) Ferrous ion oxidation in presence of ferric ion indicator xylenol orange for measurement of hydroperoxides. *Methods Enzymol.* **233,** 182–189 CrossRef